

# Investigation and comparison of analytical, numerical, and experimentally measured coupling losses for multi-step index optical fibers

Gotzon Aldabaldetrekue, Gaizka Durana, Joseba Zubia, and Jon Arrue

University of the Basque Country,  
Alda. Urquijo s/n, E-48013 Bilbao, Spain  
[gotzon.aldabaldetrekue@ehu.es](mailto:gotzon.aldabaldetrekue@ehu.es)

Hans Poisel

POF-AC, University of Applied Sciences,  
Wassertorstr. 10, D-90489 Nuremberg, Germany

María Angeles Losada

University of Zaragoza,  
María de Luna 1, E-50018 Zaragoza, Spain

**Abstract:** The aim of the present paper is to provide a comprehensive analysis of the coupling losses in multi-step index (MSI) fibres. Their light power acceptance properties are investigated to obtain the corresponding analytical expressions taking into account longitudinal, transverse, and angular misalignments. For this purpose, a uniform power distribution is assumed. In addition, we perform several experimental measurements and computer simulations in order to calculate the coupling losses for two different MSI polymer optical fibres (MSI-POFs). These results serve us to validate the theoretical expressions we have obtained.

© 2005 Optical Society of America

**OCIS codes:** (060.0060) Fiber optics and optical communications; (060.2270) Fiber characterization; (060.2300) Fiber measurements; (060.2310) Fiber optics.

---

## References and links

1. V. Levin, T. Baskakova, Z. Lavrova, A. Zubkov, H. Poisel, and K. Klein, "Production of multilayer polymer optical fibers," in *Proceedings of the Eighth International Conference on Plastic Optical Fibers and Applications-POF'99*, pp. 98–101 (Chiba (Japan), 1999).
2. K. Irie, Y. Uozu, and T. Yoshimura, "Structure design and analysis of broadband POF," in *Proceedings of the Tenth International Conference on Plastic Optical Fibers and Applications-POF'01*, pp. 73–79 (Amsterdam (The Netherlands), 2001).
3. J. Zubia, G. Aldabaldetrekue, G. Durana, J. Arrue, H. Poisel, and C. A. Bunge, "Geometric Optics Analysis of Multi-Step Index Optical Fibers," *Fiber and Integrated Optics* **23**, 121–156 (2004).
4. Mitsubishi Rayon Co., Ltd.: "Eska-Miu," URL <http://www.pofeska.com>.
5. D. Gloge, "Offset and Tilt Loss in Optical Fiber Splices," *Bell Syst. Tech. J.* **55**, 905–916 (1976).
6. T. C. Chu and A. R. McCormick, "Measurements of Loss Due to Offset, End Separation, and Angular Misalignment in Graded Index Fibers Excited by an Incoherent Source," *Bell Syst. Tech. J.* **57**, 595–602 (1978).
7. D. Marcuse, D. Gloge, and E. A. J. Marcatili, "Guiding Properties of Fibers," in *Optical Fiber Telecommunications*, S. E. Miller and A. G. Chynoweth, eds., chap. 3 (Academic Press, Inc., San Diego, California, 1979).
8. G. Keiser, *Optical Fiber Communications* (McGraw-Hill, Singapore, 1991).
9. F. L. Thiel and R. M. Hawk, "Optical waveguide cable connection," *Appl. Opt.* **15**, 2785–2791 (1976).

10. G. Jiang, R. F. Shi, and A. F. Garito, "Mode Coupling and Equilibrium Mode Distribution Conditions in Plastic Optical Fibers," *IEEE Photon. Technol. Lett.* **9**, 1128–1131 (1997).
11. Japanese Standards Association, "Test methods for attenuation of all plastic multimode optical fibers," Tech. Rep. JIS C 6863, JIS, Tokyo, Japan (1990).
12. B. Lohmüller, A. Bachmann, O. Ziemann, A. Sawaki, H. Shirai, and K. Suzuki, "The Use of LEPAS System for POF Characterization," in *11th International POF Conference 2002: Proceedings*, pp. 263–266 (Tokyo (Japan), 2002).
13. D. Marcuse, *Principles of Optical Fiber Measurements*, chap. 4 (Academic Press, Inc., London, 1981).
14. Japanese Standards Association, "Test methods for structural parameters of all plastic multimode optical fibers," Tech. Rep. JIS C 6862, JIS, Tokyo, Japan (1990).
15. A. W. Snyder and J. D. Love, *Optical Waveguide Theory* (Chapman and Hall, London, 1983).
16. J. Arrue, J. Zubia, G. Durana, J. Mateo, and M. Lopez-Amo, "Model for the propagation of pulses and mode scrambling in a real POF with structural imperfections," in *Proceedings of the Tenth International Conference on Plastic Optical Fibers and Applications-POF'01*, pp. 301–308 (Amsterdam (The Netherlands), 2001).
17. J. Zubia, H. Poisel, C.-A. Bunge, G. Aldabaldetrek, and J. Arrue, "POF Modelling," in *11th International POF Conference 2002: Proceedings*, pp. 221–224 (Tokyo (Japan), 2002).
18. T. Ishigure, M. Kano, and Y. Koike, "Which is a More Serious Factor to the Bandwidth of GI POF: Differential Mode Attenuation or Mode Coupling?" *J. Lightwave Technol.* **18**, 959–965 (2000).
19. S. E. Golowich, W. White, W. A. Reed, and E. Knudsen, "Quantitative Estimates of Mode Coupling and Differential Modal Attenuation in Perfluorinated Graded-Index Plastic Optical Fiber," *J. Lightwave Technol.* **21**, 111–121 (2003).
20. S. Savović and A. Djordjevich, "Optical power flow in plastic-clad silica fibers," *Appl. Opt.* **41**, 7588–7591 (2002).
21. S. Savović and A. Djordjevich, "Influence of numerical aperture on mode coupling in step-index plastic optical fibers," *Appl. Opt.* **43**, 5542–5546 (2004).
22. A. Ankiewicz and C. Pask, "The effects of source configuration on bandwidth and loss measurements in optical fibres," *Optical and Quantum Electronics* **15**, 463–470 (1983).
23. J. Arrue, G. Aldabaldetrek, G. Durana, J. Zubia, I. Garces, and F. Jiménez, "Design of mode scramblers for step-index and graded-index plastic optical fibres," *J. Lightwave Technol.* **23**, 1253–1260 (2005).
24. C. M. Miller and S. C. Mettler, "A Loss Model for Parabolic-Profile Fiber Splices," *Bell Syst. Tech. J.* **57**, 3167–3180 (1978).
25. S. C. Mettler, "A General Characterization of Splice Loss for Multimode Optical Fibers," *Bell Syst. Tech. J.* **58**, 2163–2182 (1979).
26. R. J. Pieper and A. Nassopoulos, "The Eikonal Ray Equations in Optical Fibers," *IEEE Trans. Educ.* **40**, 139–143 (1997).
27. D. Gloge and E. A. J. Marcatili, "Multimode Theory of Graded-Core Fibers," *Bell Syst. Tech. J.* **52**, 1563–1578 (1973).

## 1. Introduction

Multi-step index (MSI) fibres may constitute an alternative to graded-index (GI) fibres, especially to GI polymer optical fibres (GI-POF) [1, 2, 3]. They combine the manufacturing simplicity of their step-index (SI) counterparts and the higher bandwidths achievable with GI fibres. For instance, a three-layer MSI-POF with a numerical aperture ( $NA$ ) of 0.25 allows bandwidths as high as 250 MHz · 100 m, in accordance with the IEEE1394/S400 specification [4, 2]. Their good performance is due to the better stability of their refractive index profiles with ageing, and temperature and humidity fluctuations in comparison with GI fibres, thus increasing their popularity.

Mechanical misalignment is a major source of extrinsic coupling losses when joining two fibres [5, 6]. In this section we will study the three fundamental types of misalignments between fibres, namely, longitudinal separation, axial or transverse offset, and angular misalignment.

With regard to the experimental measurements, the results have been tested with two MSI-POFs of very different mode coupling rates: the "Eska-Miu" MSI-POF from Mitsubishi [4] and the "TVER" MSI-POF [1]. In every case, the calculations are valid for any kind of MSI optical fibre.

The structure of the paper is as follows. First, the theoretical calculations are presented, in order to facilitate the understanding of the behaviour of MSI fibres in terms of coupling losses.

Then, the experimental set-up is described, prior to the experimental measurements as well as the numerical computer simulations of the coupling losses for both MSI-POFs. The results obtained for these optical fibres are discussed. Finally, we summarize the main conclusions.

## 2. Theoretical analysis

MSI fibres are structurally very similar to their SI or GI counterparts: they consist of a core, a cladding that surrounds the core, and a protective jacket covering the cladding. The main difference is that the core consists of several layers of different refractive indices. The most general refractive index profile in MSI fibres can be expressed as

$$n(r) = \begin{cases} n_1; & r < \rho_1, \\ n_2; & \rho_1 \leq r < \rho_2, \\ \vdots & \\ n_N; & \rho_{N-1} \leq r < \rho_N, \\ n_{cl}; & r \geq \rho_N. \end{cases} \quad (1)$$

For the sake of simplicity, we will neglect the possible effects of the protective jacket and assume that the cladding extends to infinity. In addition, it must be pointed out that the analytical expressions do not include the Fresnel transmission coefficient, neither at the output surface of the transmitting fibre nor at the input surface of the receiving fibre. Thus, we leave aside the corresponding Fresnel reflection losses occurring at both fibre surfaces, which in the worst case can be as high as 0.4 dB and, therefore, have no significant effects on the final results. However, these should be added to the theoretical coupling losses if we pursue a more accurate estimation.

Our starting point is the calculation of the amount of source power carried by bound rays,  $P_{br}$ . As stated in Ref. [3], for a diffuse or Lambertian light source of intensity  $I_0 \cos \theta_0$  and an MSI fibre of  $N$  layers,  $P_{br}$  is given by

$$P_{br} = \pi^2 \frac{I_0}{n_0^2} \sum_{i=1}^N (\rho_i^2 - \rho_{i-1}^2) S_i = \sum_{i=1}^N P_i; \quad S_i = n_i^2 - n_{cl}^2, \quad (2)$$

and taking into account that  $S_i = NA_i^2$  in each layer,

$$P_i = \pi^2 \frac{I_0}{n_0^2} (\rho_i^2 - \rho_{i-1}^2) NA_i^2 \quad (\rho_0 = 0).$$

where  $n_i$  is the refractive index and  $\rho_i$  is the outer radius of the  $i$ -th layer.

We can rewrite the above expression as a function of the amount of source power carried by bound rays within the innermost layer,  $P_1$ :

$$\frac{P_i}{P_1} = \frac{(\rho_i^2 - \rho_{i-1}^2) NA_i^2}{\rho_1^2 NA_1^2},$$

which, in turn, allows us to express the optical power density  $W_i = P_i/A_i$  as a function of the local numerical aperture

$$\frac{W_i}{W_1} = \frac{P_i/A_i}{P_1/A_1} = \frac{[(\rho_i^2 - \rho_{i-1}^2) NA_i^2] / [\pi(\rho_i^2 - \rho_{i-1}^2)]}{[\rho_1^2 NA_1^2] / [\pi\rho_1^2]} = \frac{NA_i^2}{NA_1^2}. \quad (3)$$

The power launched into the receiving fibre for any kind of misalignment is calculated from the contribution of each layer of the transmitting fibre into each layer of the receiving fibre, taking into account the power acceptance conditions in both fibre ends. For this purpose, each portion of the accepted power in the receiving fibre is calculated from the optical power density defined in Eq. (3).

### 2.1. Longitudinal Separation and Transverse Offset

The effects of longitudinally separating the two fibre ends by a gap  $s$  and of displacing both fibre axes by a transverse offset  $d$  have been previously reported in Ref. [3], although it may be helpful for the reader to summarize them (see Tables 1 and 2).

### 2.2. Angular Misalignment

When the axes of the transmitting and receiving fibres are angularly misaligned at the joint, we are incurring losses because of the power lost outside the effective solid acceptance angle of the receiving fibre. In the case of an MSI fibre, quantifying these losses may involve cumbersome calculations, since each layer has a different numerical aperture (and, consequently, a different solid acceptance angle).

Considering the case of a uniform power distribution, we can obtain a simple and relatively accurate expression for an angular misalignment  $\alpha$ , provided that it is sufficiently small ( $\alpha \leq 10^\circ$ ), if the following assumptions are made:

- (i) the amount of power lost outside the area of the receiving fibre is neglected, and
- (ii) the losses due solely to the angular misalignment are obtained without taking into account the refraction effect (which would be equivalent to considering that fibres were spliced).

Both assumptions imply that the quasi-elliptical area projected onto the receiving fibre by the optical power emitted by each layer of the transmitting fibre does not extend beyond the circular section of the corresponding layer of the receiving fibre. Since the value of the angular misalignment is kept small, the gap created between both fibre ends is not large enough to allow a significant deviation in the overlapping areas, irrespective of whether we have neglected or not the refractive index difference between fibre and air.

As stated in Refs. [5] and [7], in the case of the refractive index profiles of the MSI fibres considered above, the angular misalignments can be treated in the same way as the transverse offsets (see the appendix for further explanation). In the calculation of the coupling loss due to a transverse offset, the power coupled into the receiving fibre was obtained by integrating the optical power density given by Eq. (3) separately over the overlapping areas of both transmitting and receiving fibres [8, 3]. By means of a similar reasoning, the coupling loss for the angular misalignment  $L_{AM}$  can be easily found as

$$L_{AM} = -10 \log \frac{2}{\pi \sum_{i=1}^N (\rho_i^2 - \rho_{i-1}^2) NA_i^2} \left\{ \sum_{i=2}^j NA_i^2 \delta_i + NA_1^2 \rho_1^2 \left[ \arccos q_1 - q_1 (1 - q_1^2)^{1/2} \right] \right\}, \quad (4)$$

where

$$\delta_i = \rho_i^2 \arccos q_i - \rho_{i-1}^2 \arccos q_{i-1} + \rho_{i-1}^2 q_{i-1} (1 - q_{i-1}^2)^{1/2} - \rho_i^2 q_i (1 - q_i^2)^{1/2},$$

$q_i$  stands for

$$q_i = \frac{n_i \sin \alpha}{2 (n_i^2 - n_{cl}^2)^{1/2}},$$

and  $j$  is an integer value that satisfies

$$\frac{NA_{j-1}}{n_{j-1}} \leq \frac{\sin \alpha}{\sqrt{2}} < \frac{NA_j}{n_j}.$$

Table 1. Analytical expression of the coupling loss  $L_{LS}$  for a longitudinal separation  $s$  for MSI fibres. (After Ref. [3].)

$$L_{LS} = -10 \log \frac{P_{ac}}{P_{br}},$$

which is valid for  $s \leq \rho_1 / \tan \theta_2$ , so that a uniform optical power density can still be assumed, and where

$$P_{ac} = P_1^1 + \sum_{i=2}^p P_1^i + \sum_{j=2}^q P_j^1 + \sum_{j=2}^N \sum_{i=u}^v P_j^i,$$

and

$$P_1^1 = \frac{\pi^2 I_0}{n_0^2} \frac{NA_1^2}{(\rho_1 + s \tan \theta_1)^2} \rho_1^4,$$

$$P_{j \geq 2}^1 = \frac{\pi^2 I_0}{n_0^2} \frac{\rho_1^2 NA_j^2}{(\rho_1 + s \tan \theta_1)^2} \left[ \min \left\{ \rho_j^2, (\rho_1 + s \tan \theta_1)^2 \right\} - \rho_{j-1}^2 \right],$$

$$P_1^{i \geq 2} = \frac{\pi^2 I_0}{n_0^2} \frac{NA_i^2}{\left\{ 1 + \frac{2s \tan \theta_i}{\rho_i - \rho_{i-1}} \right\}} \left[ \rho_1^2 - (\rho_{i-1} - s \tan \theta_i)^2 \right],$$

$$P_{j \geq 2}^{i \geq 2} = \begin{cases} \frac{\pi^2 I_0}{n_0^2} \frac{NA_j^2}{\left\{ 1 + \frac{2s \tan \theta_i}{\rho_i - \rho_{i-1}} \right\}} \left[ \min \left\{ \rho_j^2, (\rho_i + s \tan \theta_i)^2 \right\} - \max \left\{ \rho_{j-1}^2, (\rho_{i-1} - s \tan \theta_i)^2 \right\} \right] & \text{if } i < j, \\ \frac{\pi^2 I_0}{n_0^2} \frac{NA_i^2}{\left\{ 1 + \frac{2s \tan \theta_i}{\rho_i - \rho_{i-1}} \right\}} \left[ \min \left\{ \rho_j^2, (\rho_i + s \tan \theta_i)^2 \right\} - \max \left\{ \rho_{j-1}^2, (\rho_{i-1} - s \tan \theta_i)^2 \right\} \right] & \text{if } i \geq j. \end{cases}$$

The integers  $p$ ,  $q$ ,  $u$  and  $v$  are the limits of integration, satisfying

$p = \max \{ \text{all possible values of } k \}$  so that

$$\rho_{k-1} - s \tan \theta_k < \rho_1; \quad p = 2 \dots N,$$

$q = \max \{ \text{all possible values of } k \}$  so that

$$\rho_{k-1} \leq \rho_1 + s \tan \theta_1 < \rho_k; \quad q = 2 \dots N,$$

$u = \min \{ \text{all possible values of } k \}$  so that

$$(\rho_k + s \tan \theta_k \geq \rho_{j-1}) \text{ and } (\rho_{k-1} - s \tan \theta_k < \rho_j); \quad 2 \leq u \leq v \leq N,$$

$v = \max \{ \text{all possible values of } k \}$  so that

$$(\rho_k + s \tan \theta_k \geq \rho_{j-1}) \text{ and } (\rho_{k-1} - s \tan \theta_k < \rho_j); \quad 2 \leq u \leq v \leq N.$$

Table 2. Analytical expression of the coupling loss  $L_{TO}$  for a transverse offset  $d$  for MSI fibres. (After Ref. [3].)

$$L_{TO} = -10 \log \frac{2 \left\{ \sum_{i=j+1}^N NA_i^2 A_i + NA_j^2 \left[ \rho_j^2 \arccos \frac{d}{2\rho_j} - \frac{d}{2} (\rho_j^2 - d^2/4)^{1/2} \right] \right\}}{\pi \sum_{i=1}^N (\rho_i^2 - \rho_{i-1}^2) NA_i^2},$$

where

$$A_i = \rho_i^2 \arccos \frac{d}{2\rho_i} - \rho_{i-1}^2 \arccos \frac{d}{2\rho_{i-1}} + \frac{d}{2} \left\{ (\rho_{i-1}^2 - d^2/4)^{1/2} - (\rho_i^2 - d^2/4)^{1/2} \right\},$$

and  $j$  is an integer value that satisfies

$$\rho_{j-1} \leq d/2 < \rho_j.$$

It is straightforward to show that, by taking  $N = 1$ , Eq. (4) reduces to the coupling loss for an SI fibre

$$L_{AM} \Big|_{N=1} = -10 \log \frac{2}{\pi} \left\{ \arccos q_1 - q_1 (1 - q_1^2)^{1/2} \right\},$$

yielding similar results to those obtained by Thiel *et al.* in Ref. [9].

### 3. Experiment

Figure 1 shows the experimental set-up employed to measure the coupling losses of MSI poly-methyl-methacrylate PMMA-based POFs due to mechanical misalignments.

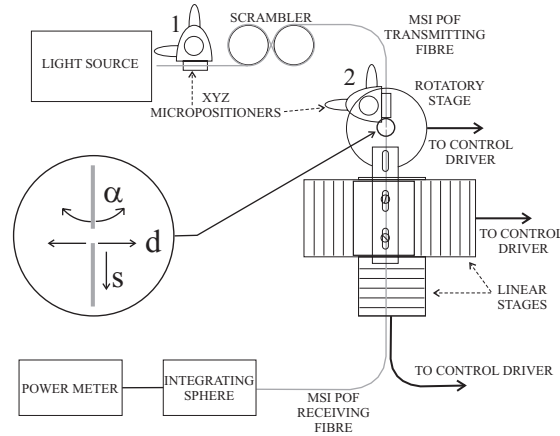


Fig. 1. Experimental set-up used to measure coupling losses of MSI-POFs.

The transmitting fibre stands on a rotatory stage, whereas the receiving fibre is fixed to one of the two linear stages which are placed perpendicularly to each other. The system is fully

automated, and it allows the measurement of angular misalignments, longitudinal separations and transverse offsets, respectively. In all the measurements, the length of the transmitting and receiving fibres was 2 m.

The measurements have been performed using different configurations for the light source: (1) a green LED, (2) a red laser diode ( $\lambda = 662.5$  nm) followed by an objective lens in order to select a certain numerical aperture at the input surface of the transmitting fibre (specifically,  $NA_{input} = 0.1$  and  $0.65$ ), and (3) a  $0.1$ -NA light source combined with a scrambler. This device consists of an 8-shaped section of the transmitting fibre that contributes by its mode mixing to a faster reaching of the so-called equilibrium mode distribution (EMD), independently of the light source [10]. The two cylinders in such a scrambler were of 42 mm in diameter and the distance between centres was 45.5 mm (in agreement with the standard JIS for conventional SI-POF [11]). The light that exits the receiving fibre is collected by an Ulbricht integrating sphere.

The power coupling from the source to the input surface of the transmitting fibre was optimized using the micropositioner No. 1 shown in Fig. 1 (for the LED source, the fibre was directly attached to the source). Each set of measurements began by establishing the position  $d = s = \alpha = 0$ , for which the power output from the receiving fibre was maximized.  $s$  stands for longitudinal separation,  $d$  for transverse offset, and  $\alpha$  for angular misalignment. This position was achieved by using both the linear stages and the micropositioner No. 2 shown in Fig. 1.

For each of the light source configurations described above, the coupling loss measurements were carried out sequentially as follows: first of all, coupling loss against longitudinal separation measurements were taken for different transverse offsets. Next, coupling loss against transverse offset measurements were recorded for different longitudinal separations; and finally, coupling loss against angular misalignment was measured for different longitudinal separations as well as for different transverse offsets. The near- and far-fields of the transmitting fibre were measured with the Hamamatsu LEPAS system [12]. The step size for each set of measurements was different:  $100 \mu\text{m}$  for longitudinal separations,  $30 \mu\text{m}$  for transverse offsets, and  $0.3^\circ$  for angular misalignments.

#### 4. Results and discussion

Coupling loss measurements were taken for two different MSI-POFs: the Eska-Miu fibre from Mitsubishi [4], and the MSI-POF from TVER [1]. The former has three layers, whereas the latter has four. The physical dimensions of the different layers are summarized in Table 3.

Table 3. Physical dimensions of the different layers (outer radii in mm).

	Layer 1	Layer 2	Layer 3	Layer 4
Eska-Miu	0.25	0.35	0.38	–
TVER	0.16	0.23	0.27	0.33

It must be pointed out that the first layer of the Eska-Miu fibre is quite thick, whereas the third one is extremely thin, in contrast to the similar but rather irregular layer thicknesses of the TVER fibre. This can be observed in Fig. 2, where cross-section photographs of each MSI-POF (Figs. 2(a) and 2(b)) together with their respective refractive index profiles (Figs. 2(c) and 2(d)) are shown. The refractive index profiles were measured with the aid of the inverse near-field method [13, 14]. The implications of having such particular geometric arrangements and refractive index profiles for the results obtained will be analyzed in subsequent subsections.

In a typical SI PMMA-POF the refractive index  $n$  is 1.492 in the core and a lower value in the cladding ranging between 1.40 and 1.42. For the analytical calculations and the numerical

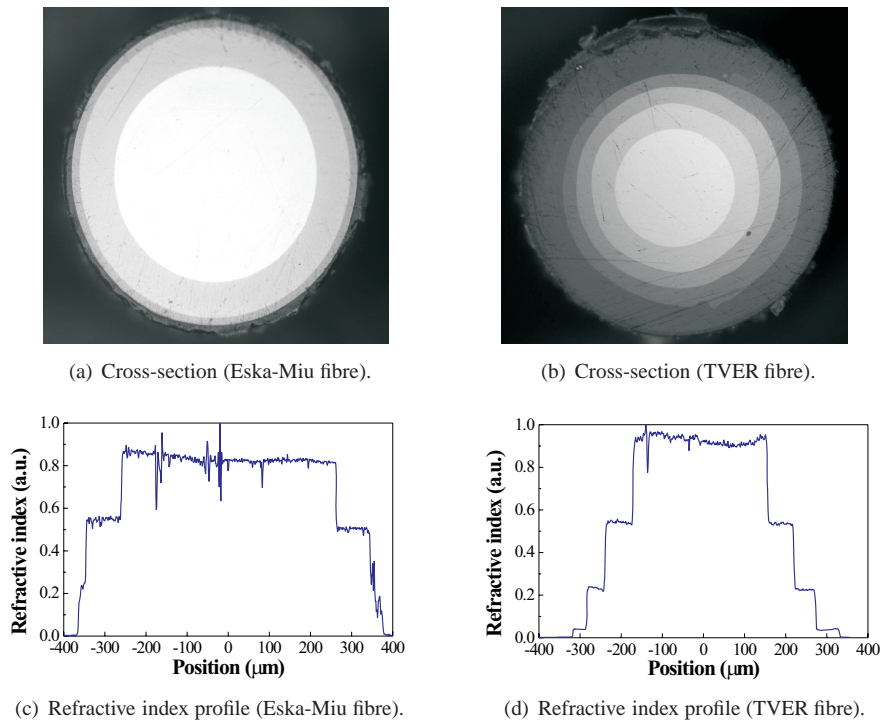


Fig. 2. Cross-section photographs of the MSI-POFs and their respective refractive-index profiles.

computer simulations, we have taken the value of 1.492 as the refractive index of the innermost layer ( $n_1$ ), considering a value of 1.402 as the refractive index of the cladding ( $n_{cl}$ ). The refractive indices of the remaining layers in between are adjusted according to the measured refractive index profiles in Fig. 2 relative to the extreme values  $n_1$  and  $n_{cl}$ . We have chosen the ray-tracing method for the computer simulations.

As for the launching conditions, the computer simulations reproduce accurately the different types of light source employed in the experimental measurements. We have utilized two hypothetical light sources. One of them emits a Gaussian near-field power distribution characterized by a full width at half maximum (FWHM) of  $80\ \mu\text{m}$  and provides a uniform mode distribution (UMD) within the numerical apertures  $NA_{input} = 0.1$  or  $0.65$ . The other one is a lambertian LED source that covers the whole input surface of the transmitting fibre, the lambertian exponent  $s$  for the angular distribution being 1. We have launched approximately 200000 rays into the Eska-Miu and the TVER fibres. This number ranges between an upper boundary delimited by the total number of modes that can propagate within the fibres and a lower boundary to ensure sufficiently smooth and accurate results. The former is calculated from the waveguide parameter  $V$  [15].

For convenience, the analytical results have been superimposed on the graphs showing the numerical results obtained for the case of a UMD within an input numerical aperture of  $NA_{input} = 0.65$  (which ensures that the launched rays will fill the effective solid acceptance angle of the transmitting fibre). In principle, both sets of results should be similar.

It is worthy of remark that the numerical results obtained from the simulations correspond to ideal fibres, whereas the experimental measurements deal with real fibres. In the latter, intrin-

sic physical phenomena can give rise to many different effects that can have an influence on the fibre transmission characteristics affecting coupling losses. (To some extent it is possible to simulate these effects by deflecting the direction of the light rays from that predicted by Snell's law by using an appropriate probability distribution function. Previous works have successfully demonstrated its feasibility in SI-POFs, as discussed in Refs. [16] and [17], but its implementation in MSI fibres is much more elaborate and complicated. For this reason, in this paper we will only consider ideal fibres when performing numerical simulations.)

#### 4.1. Previous considerations of the mode coupling effects

Among these effects, differential mode attenuation (DMA) and mode coupling have a great influence on the performance of the fibre [10, 18, 19, 20]. We believe that mode coupling is much more important in MSI-POFs than the DMA, in view of the results that we present below. The former arises from intrinsic perturbation effects, such as microscopic anomalies in the fibre core, irregularities in the core-cladding interface, or inhomogeneities in the refractive index profile. In our particular case, the influence of the numerical aperture on the coupling rate has proved to be negligible because of the short length of the measured fibres, so the coupling coefficient can be considered as the dominant parameter in the mode coupling process [21].

In order to assess the importance that mode coupling has on each MSI-POF, we have plotted, on Figs. 3 and 4, the experimental near- and far-fields of the transmitting fibres for both MSI-POFs and for the first three launching configurations mentioned (namely, the red laser diode followed by an objective with  $NA_{input} = 0.1$ , the same light source followed by another objective with  $NA_{input} = 0.65$ , and the green LED). Likewise, the experimental near- and far-fields obtained using a 0.1-NA light source in combination with a scrambler in the shape of an 8, yielding an angular emission pattern similar to that of the EMD, are shown in Fig. 5.

On the one hand, the different angular emission patterns obtained from the far-fields in the case of the Eska-Miu fibre (as shown in Figs. 3(b), 3(d) and 3(f)) suggest a very low rate of mode coupling, because of the strong dependence of the results on the launching conditions. In contrast, Figs. 4(b), 4(d) and 4(f) indicate that there is no such a dependence on the launching conditions in the case of the TVER fibre, which is a clear sign of a strong mode coupling effect. This can be concluded from the similarities between these far-fields and those obtained using the scrambler (which speeds up the process of achieving the EMD), as shown in Fig. 5(d). This fact can be explained by the many structural imperfections of the TVER fibre, its quality being much poorer than that of the Eska-Miu fibre (as becomes apparent in Figs. 2(a) and 2(b)). As a result of such imperfections the mode coupling rate is higher.

This is the main reason for having practically the same coupling loss results for the TVER fibre regardless of the source configuration employed in the experimental measurements, as will be seen below [22]. Being unable to draw any meaningful conclusions from the experimental measurements of the TVER fibre, the computer simulations have proved to be a very valuable tool in order to compare the effects of the characteristics of each fibre on their performance in terms of coupling losses.

On the other hand, the near-field of the Eska-Miu fibre from Fig. 3(a) shows that, even though light power has been launched onto a very small spot and within an input numerical aperture  $NA_{input} = 0.1$  (ensuring that ideally no refraction takes place to the outermost layers), there is a small fraction of power collected by the second and third layers (although it is virtually negligible in this last one). This clearly suggests that there is some power transfer from lower to higher order modes. For the source configurations using a 0.65-NA source and a 0.1-NA source combined with an 8-shaped scrambler (see Figs. 3(c) and 5(a), respectively) this effect is not so apparent, because part of the light power is refracted to outer layers due to the high input numerical aperture in the former case and to the curvature of the bent fibre section in

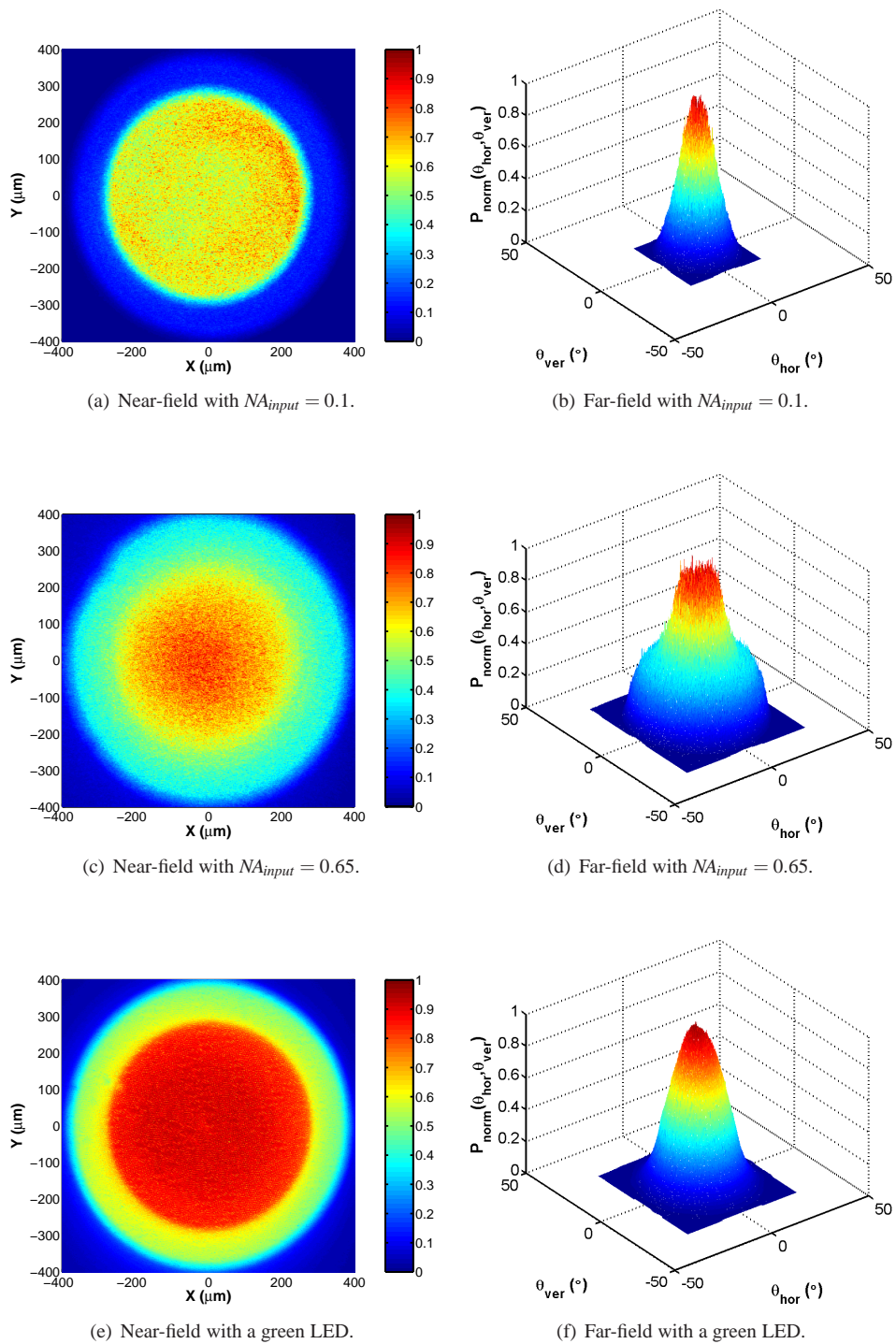
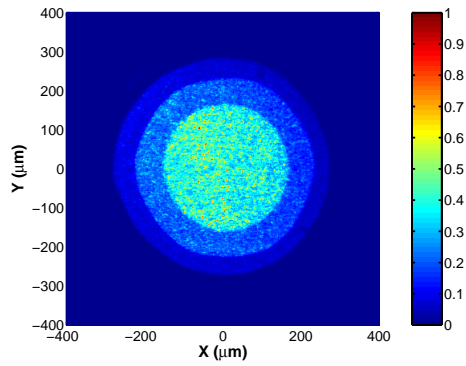
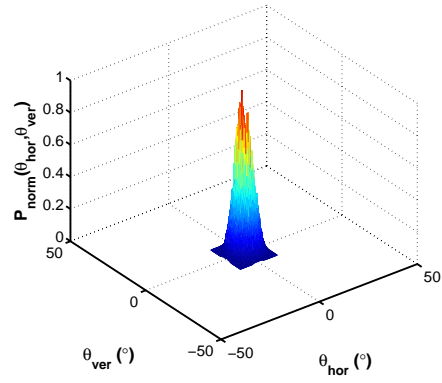


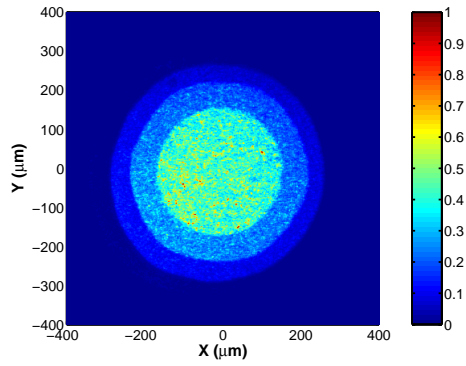
Fig. 3. Eska-Miu fibre. Experimental near- and far-fields of the transmitting fibre for different source configurations used in the measurements.



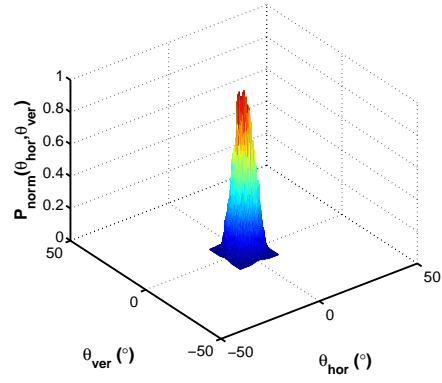
(a) Near-field with  $NA_{input} = 0.1$ .



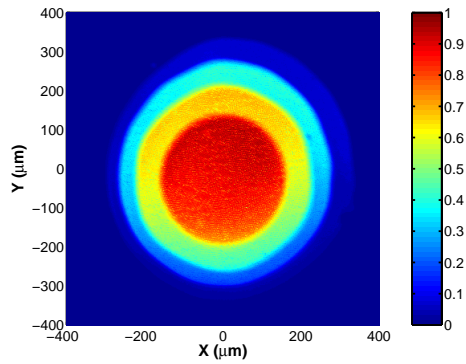
(b) Far-field with  $NA_{input} = 0.1$ .



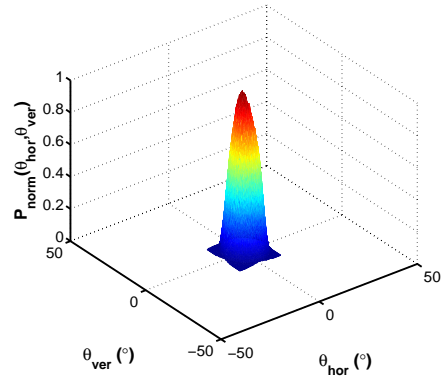
(c) Near-field with  $NA_{input} = 0.65$ .



(d) Far-field with  $NA_{input} = 0.65$ .



(e) Near-field with a green LED.



(f) Far-field with a green LED.

Fig. 4. TVER fibre. Experimental near- and far-fields of the transmitting fibre for different source configurations used in the measurements.

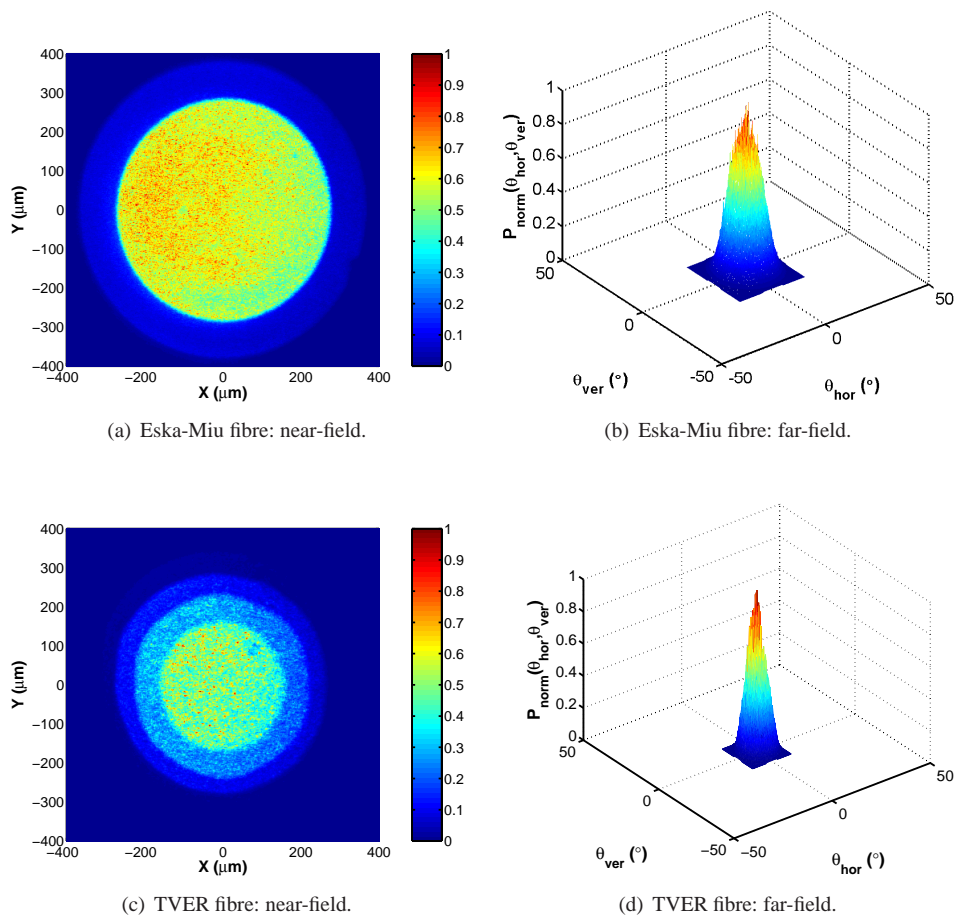


Fig. 5. Experimental near- and far-fields of the transmitting fibre with an 8-shaped scrambler used in the measurements for the Eska-Miu and TVER fibres ( $NA_{\text{input}} = 0.1$ ).

the latter. The case corresponding to the green LED excitation is an exception in itself, since it covers the whole input surface of the transmitting fibre and therefore the effects of mode coupling on the near-field shown in Fig. 3(e) become masked. The same conclusions apply to the TVER fibre.

Since our numerical simulations involve only ideal fibres without real perturbation of the propagation mechanisms of the light power, the fraction of power coupled to the outer layers is null or very small, depending on the launching conditions. It is null when rays are launched from the 0.1- $NA$  hypothetical source, and very small in the case of having launched rays from the 0.65- $NA$  hypothetical source, as can be deduced from the near- and far-fields shown in Figs. 6 and 7, even though the measured coherence length for the latter is of approximately 5 mm [23].

As a consequence, there can be significant deviations between the experimental and simulated results for the aforementioned source configurations. In order to determine the exact influence on the coupling loss measurements, we have performed several simulations using the same source configurations but this time covering the whole input surface of the transmitting

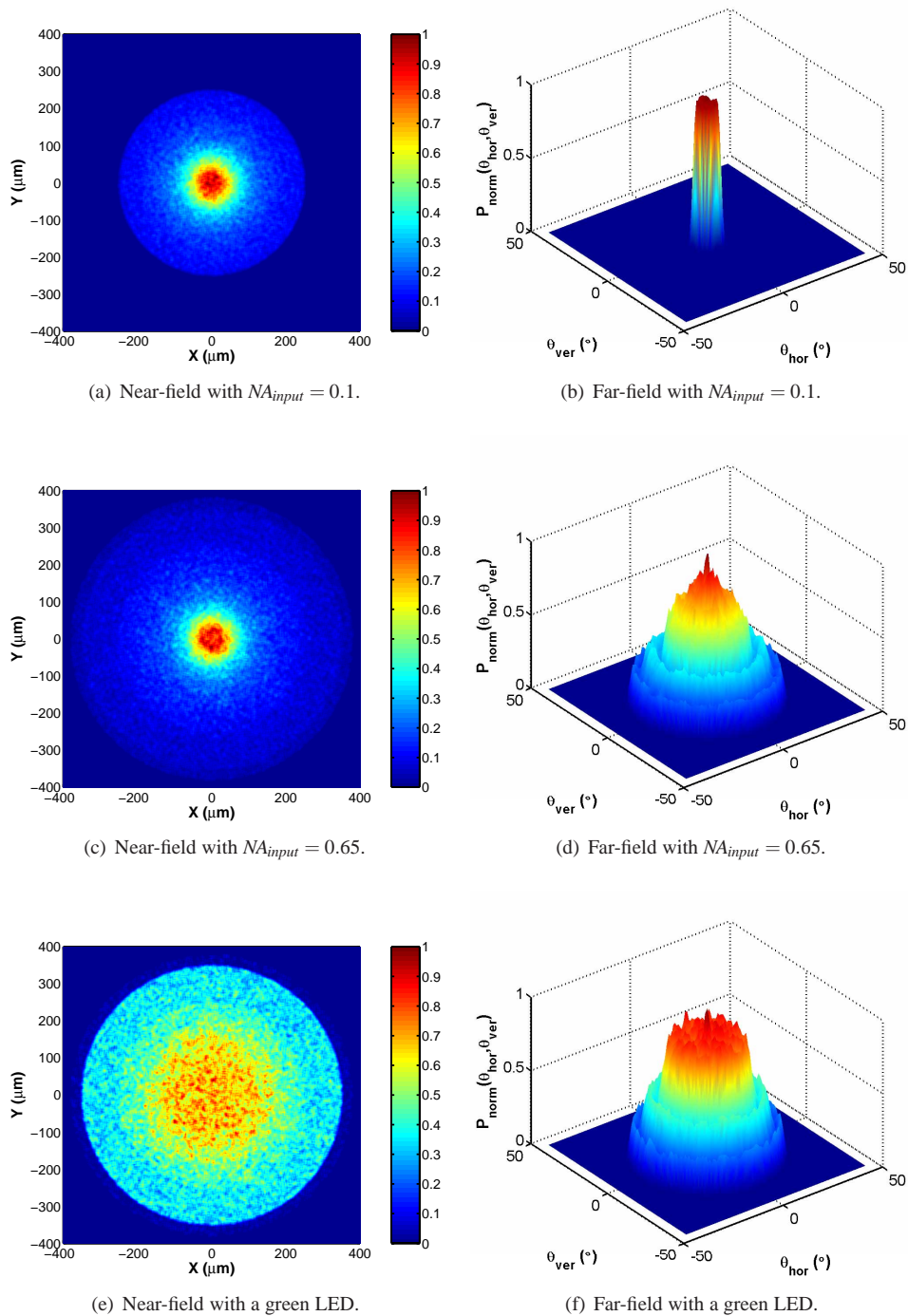


Fig. 6. Eska-Miu fibre. Near- and far-fields of the transmitting fibre for different source configurations used in the numerical computer simulations.

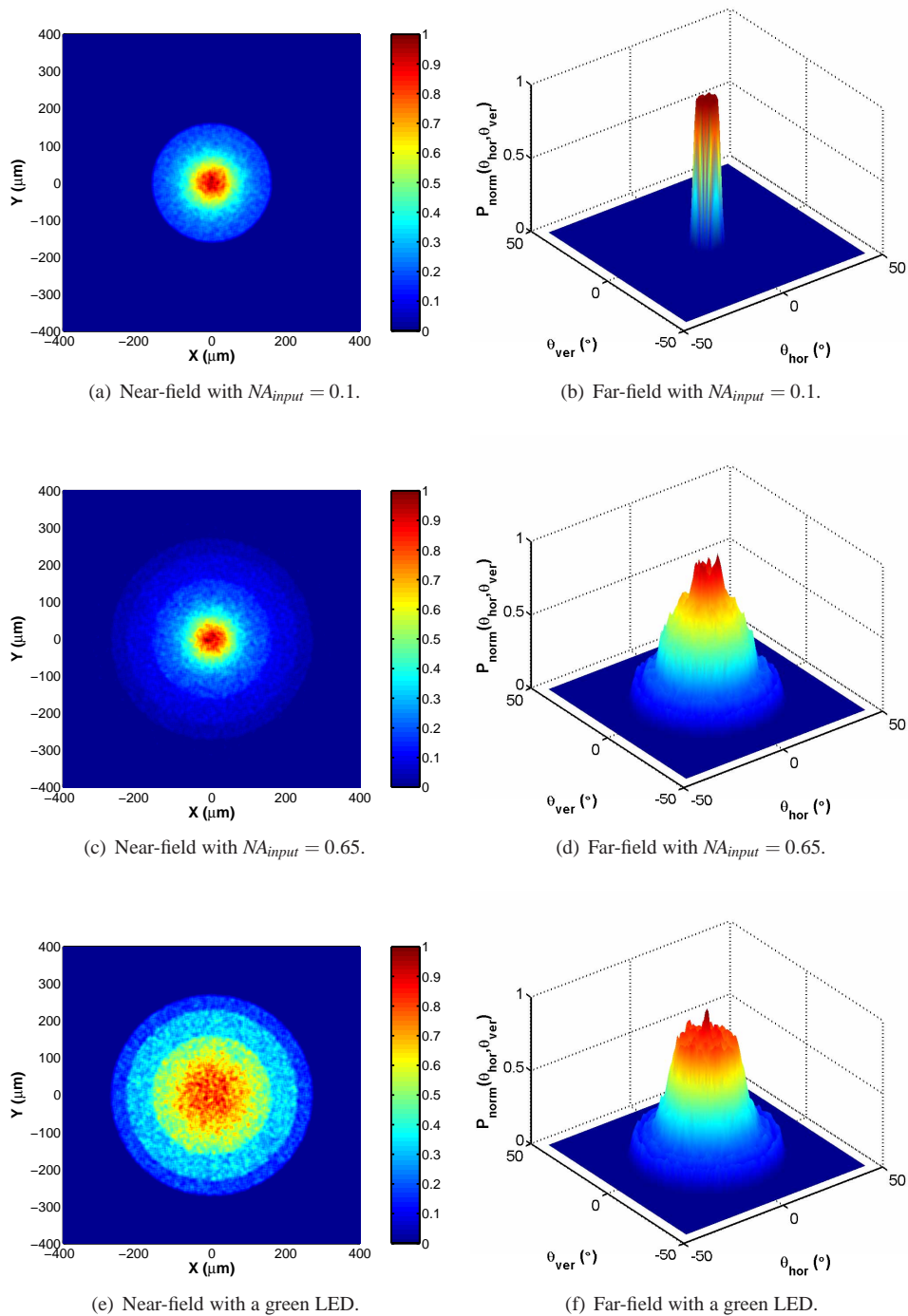


Fig. 7. TVER fibre. Near- and far-fields of the transmitting fibre for different source configurations used in the numerical computer simulations.

fibre for both MSI-POFs (shown in the insets). The implication of such measurements will be discussed in the following subsections.

#### 4.2. Longitudinal separation

We present below the experimental and numerical results for the coupling losses (in dB units) against the normalized longitudinal separation  $s/R_{outer}$  corresponding to different transverse offsets ( $R_{outer}$  denotes the outermost layer of the fibre, 0.38 mm for the Eska-Miu fibre or 0.33 mm for the TVER one). Figure 8 shows the results obtained for the Eska-Miu fibre, whereas those for the TVER fibre are presented in Fig. 9. Different plots correspond to the different source configurations explained above (see section 3). The analytical results for the Eska-Miu and the TVER fibres are shown superimposed on Figs. 8(d) and 9(d), respectively. Notice that the validity of the analytical formula reproduced in Table 1 is limited to the region where  $s \leq \rho_1 / \tan \theta_2$ , which has a value  $s/R_{outer} = 1.4389$  for the Eska-Miu fibre and  $s/R_{outer} = 1.1595$  for the TVER fibre. The insets in Figs. 8(b), 8(d), 9(b) and 9(d) show the numerical results that would be obtained using the same launching conditions but covering the whole input surface of the transmitting fibre. Additionally, the experimental results for both MSI-POFs with an 8-shaped mode scrambler (indicative of the results that would be obtained under EMD conditions) are plotted on Fig. 10.

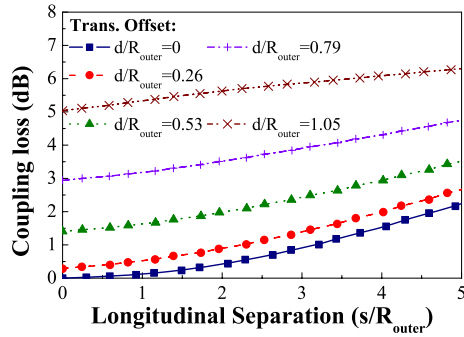
At first sight, it can be seen that the analytical expressions show fairly pessimistic values for both fibres, in contrast to the experimental and numerical results in the absence of any transverse offset ( $d/R_{outer} = 0$ ), so we must conclude that the former lead to very conservative results in terms of coupling efficiency.

On the one hand, it is found that the numerical results for the Eska-Miu fibre are in good agreement with the experimental ones. Slightly worse results if the simulations are performed under overfilled mode distribution conditions can be expected from direct comparison between the sets of Figs. 8(c) and 8(d), and Figs. 8(e) and 8(f) [24, 25]. However, the numerical results in Fig. 8(b), if compared to the experimental measurements obtained using a 0.1-NA light source (see Fig. 8(a)), suggest just the opposite behaviour under underfilled mode distribution conditions. Indeed, the coupling losses are higher in the experimental measurements than in the numerical simulations, even if we consider that the source covers the whole fibre surface, both for longitudinal separations at a constant transverse offset and vice versa. The main responsible for such a behaviour is mode coupling, since:

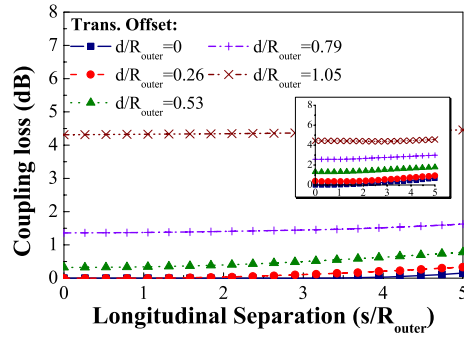
- (i) it gives rise, at the exit of the transmitting fibre, to a cone of radiation of higher divergence than it should ideally have (see subsection 4.1 and Figs. 3(b) and 6(b) above), which results in higher losses as the separation between fibre ends increases;
- (ii) it causes more light power to propagate in the outermost layers (see Figs. 3(a) and 6(a)) and, therefore, the effects on the coupling loss of displacing both fibres transversely are more dramatic. In this sense, the numerical results shown in the inset, which correspond to the case in which the source covers the whole fibre surface, are more similar to the experimental results, provided that intermediate transverse offset values are considered.

In any case, both experimental and numerical results for the Eska-Miu fibre suggest that, as longitudinal separation increases, the dependence of coupling losses on launching conditions starts to be noticeable (which is also indicative of the lack of strong mode coupling effect in this particular MSI-POF). For example, from Figs. 8(a) and 8(c), which correspond to input numerical apertures of 0.1 and 0.65 respectively, it can be observed that the coupling loss increases with the input numerical aperture for large longitudinal separations.

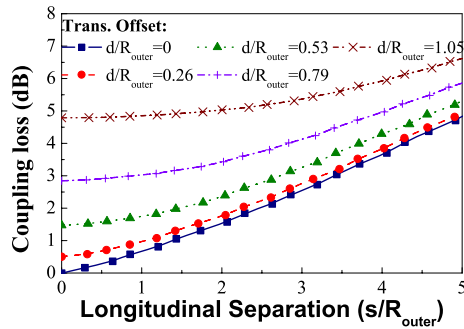
On the other hand, there is not such a dependence on launching conditions in the case of the TVER fibre because of the high rate of mode coupling caused by the structural irregularities,



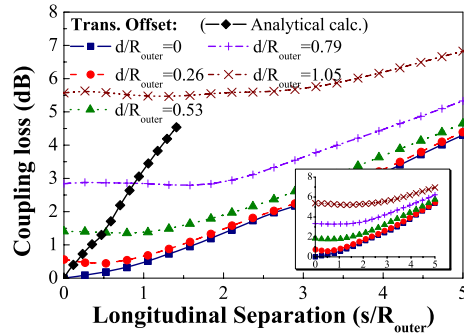
(a) Experimental results with  $NA_{input} = 0.1$ .



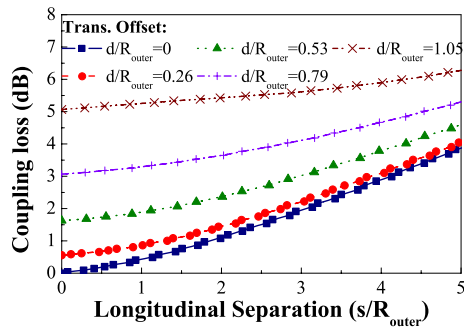
(b) Numerical results with  $NA_{input} = 0.1$ .



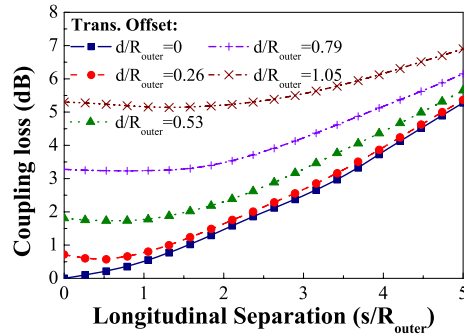
(c) Experimental results with  $NA_{input} = 0.65$ .



(d) Numerical results with  $NA_{input} = 0.65$ .

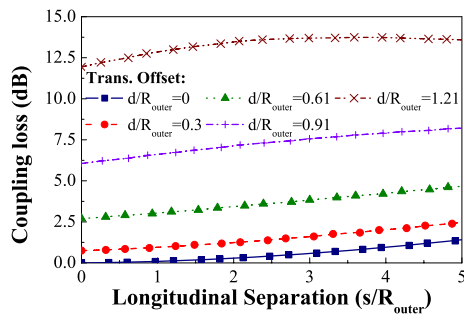


(e) Experimental results with a green LED.

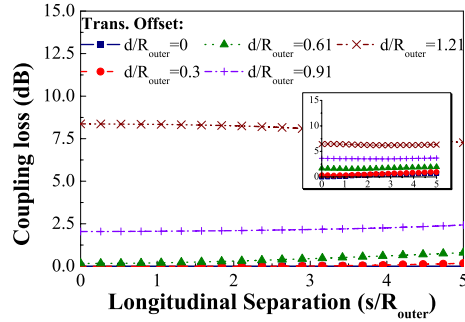


(f) Numerical results with a green LED.

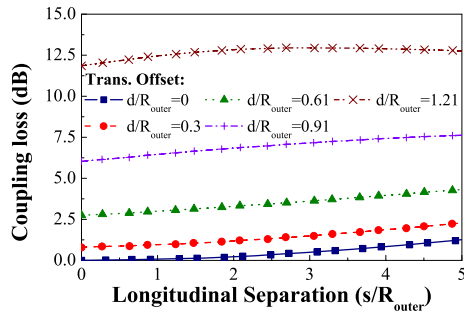
Fig. 8. Eska-Miu fibre. Coupling loss against normalized longitudinal separation  $s/R_{outer}$  for various transverse offsets and for different source configurations. Experimental and numerical results. The insets correspond to the results obtained when the source covers the whole input surface of the transmitting fibre. The analytical results denoted by  $\blacklozenge$  are shown superimposed on the numerical results obtained with  $NA_{input} = 0.65$ .



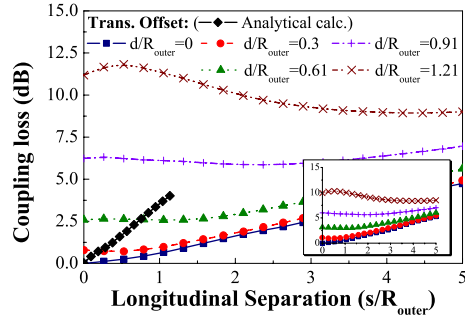
(a) Experimental results with  $NA_{input} = 0.1$ .



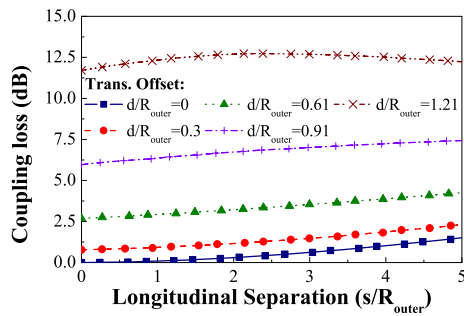
(b) Numerical results with  $NA_{input} = 0.1$ .



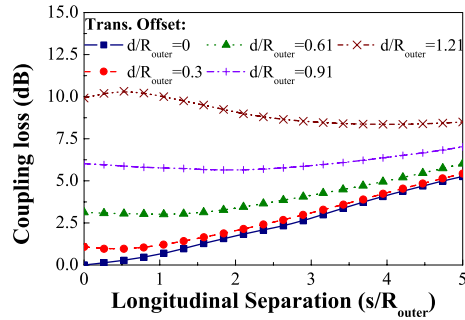
(c) Experimental results with  $NA_{input} = 0.65$ .



(d) Numerical results with  $NA_{input} = 0.65$ .



(e) Experimental results with a green LED.



(f) Numerical results with a green LED.

Fig. 9. TVER fibre. Coupling loss against normalized longitudinal separation  $s/R_{outer}$  for various transverse offsets and for different source configurations. Experimental and numerical results. The insets correspond to the results obtained when the source covers the whole input surface of the transmitting fibre. The analytical results denoted by  $\blacklozenge$  are shown superimposed on the numerical results obtained with  $NA_{input} = 0.65$ .

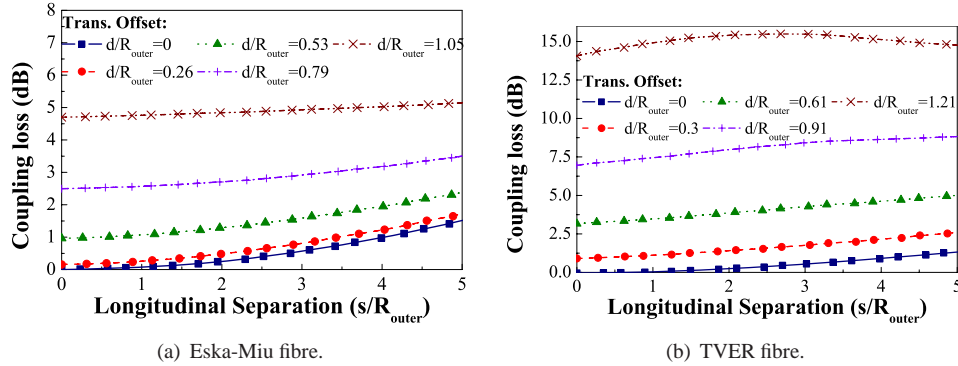


Fig. 10. Coupling loss against normalized longitudinal separation  $s/R_{outer}$  for various transverse offsets and using an 8-shaped scrambler in the transmitting fibre ( $NA_{input} = 0.1$ ). Experimental results obtained for the Eska-Miu and TVER fibres.

as explained in subsection 4.1. For this reason, the numerical results for the TVER fibre do not fit the experimental ones. However, we can draw important conclusions by comparing the numerical results obtained for the Eska-Miu and the TVER fibres (sets of Figs. 8(b) and 9(b), Figs. 8(d) and 9(d), and Figs. 8(f) and 9(f)), or the experimental results of Figs. 10(a) and 10(b), which correspond to measurements performed under nearly EMD conditions.

In this way, it can be firstly observed that in the absence of any transverse offset, coupling losses are slightly higher for the Eska-Miu fibre than for the TVER one as longitudinal separation increases. Equivalently, for a certain coupling loss, the allowed longitudinal separation is higher for the TVER fibre than for the Eska-Miu one. For instance, when utilizing a 0.1- $NA$  light source in combination with an 8-shaped scrambler in the transmitting fibre, we have measured a 3 dB coupling loss for longitudinal separations  $s/R_{outer} = 8.29$  in the case of the TVER fibre and only 7.38 in the case of the Eska-Miu one. This difference is more subtle in the numerical results, since they have been ideally obtained using the same launching conditions and normalized separations. Thus, the effects of longitudinal separations on coupling losses are mainly due to the divergence of the cone of radiation defined by the local numerical aperture, which also depends on the refractive index profile of the fibre. As a matter of fact, it is clear from Figs. 5(b) and 5(d) that the experimental cone of radiation at the exit of the transmitting Eska-Miu fibre has a higher divergence than that from the TVER one.

Secondly, the coupling losses are much higher for the TVER fibre than for the Eska-Miu one when there is a transverse offset, which is easy to understand if we refer again to the near- and far-fields of both fibres. For instance, Figs. 5(c) and 5(d) show that, irrespectively of the source configuration, in the case of the TVER fibre the energy is concentrated mainly within the innermost layers. This distribution of power is a direct consequence of the refractive index profile exhibited by the TVER fibre, as explained in the following. At the exit of the transmitting fibre a cone of radiation whose cross-section area at  $s/R_{outer} = 0$  can be defined in terms of the surface area of the innermost layers. At the same time, the rest of the surface area of the fibre covered by the two outermost layers is still significant, even though such layers have the lowest numerical apertures. In the case of the Eska-Miu fibre (see Figs. 5(a) and 5(b)), the cone of radiation of the transmitting fibre is wider in its base due to its very thick innermost layer, but the outermost one, that is, the layer which collects the lowest fraction of emitted power, is extremely thin, which implies less sensitivity of coupling losses to transverse offsets for small longitudinal separations.

All in all, low coupling losses require a very small transverse offset  $d$ , whose effects will be analyzed in more detail in the following subsection. As an introduction, let us first consider the longitudinal separation alone, and compare it with the transverse offset alone. In the case of the Eska-Miu fibre illuminated by a 0.1- $NA$  red laser diode through an 8-shaped scrambler (Fig. 10(a)), we can see that 1 dB of coupling loss is achieved when the gap between both ends is  $s/R_{outer} = 4$ , or when the transverse offset is only  $d/R_{outer} = 0.53$ . The TVER fibre presents higher coupling losses than the Eska-Miu one even with moderate transverse offsets ( $d \sim R_{outer}$ ). For example, in Fig. 10(b), for a transverse offset  $d/R_{outer} = 0.91$  and no longitudinal separation coupling losses are approximately 7 dB, whereas only 4.7 dB in the case of the Eska-Miu fibre for  $d/R_{outer} = 1.05$ , which is an even higher transverse offset than 0.91.

### 4.3. Transverse Offset

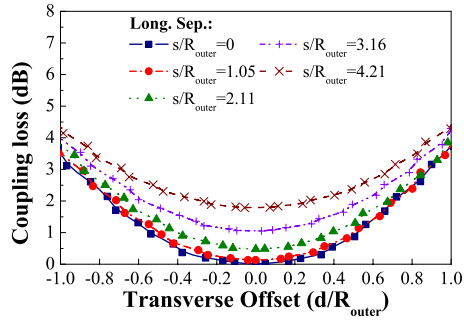
We present now experimental and numerical results for coupling losses as a function of the normalized offset  $d/R_{outer}$  for different longitudinal separations and source configurations, as explained in section 3. Again, the analytical results for both MSI-POFs are shown superimposed on the numerical results for a 0.65- $NA$  source. The insets show, in addition, the numerical results that would be obtained if the same launching conditions were employed, but this time making use of a source covering the whole input surface of the transmitting fibre.

First of all, it can be seen in Fig. 11 (Eska-Miu fibre), Fig. 12 (TVER fibre), and Fig. 13 (experimental results obtained for both MSI-POFs with an 8-shaped scrambler), that even small offsets result in high coupling losses.

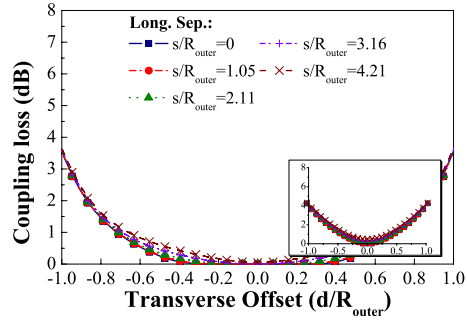
By comparing the set of experimental and numerical results in the absence of any longitudinal separation between fibre ends ( $s/R_{outer} = 0$ ) with the analytical coupling loss, we can observe that the latter shows slightly higher values. This is due to its conservative nature, since it involves overfilled mode distribution conditions. Even so, it is clear that they are in excellent agreement.

With regard to the similarities between the experimental and numerical results, we can conclude that the simulations using a source covering the whole input surface of the transmitting fibre reproduce the experimental measurements in a more accurate fashion than those using a source emitting a very small near-field injection spot. The results are plotted on the corresponding insets. This is not the case for those experimental results obtained for the TVER fibre, which were reported in previous subsections not to depend on the launching conditions due to stronger mode coupling. The similarity is even greater when light sources of low input numerical apertures ( $NA_{input} = 0.1$ ) are employed. This is because the fraction of power coupled to the outermost layers is null or practically negligible, depending on the input numerical aperture (e.g., in our analysis  $NA_{input} = 0.1$  or 0.65). As a consequence, the numerical coupling loss only starts to become noticeable when the amount of transverse displacement between both fibre ends is large enough for the innermost layer of the transmitting fibre to be able to radiate outside the input surface of the receiving one. This behaviour can be deduced from the flat curves exhibited by Figs. 11(b) and 12(b) in the region of small transverse offsets.

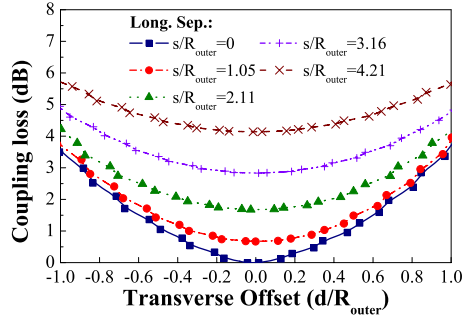
For a transverse offset, in the same way as happened with a longitudinal separation, it is remarkable that coupling loss increases with the input numerical aperture in the case of the Eska-Miu fibre (Figs. 11(a) and 11(c)). This could be explained assuming that an increase in the input numerical aperture involves a redistribution of the light power that reduces the power density in any given cross-section area of the radiation cone from the transmitting fibre (in other words, the aperture of the cone of radiation increases with the input numerical aperture). This behaviour is not observed in the case of the TVER fibre, since the experimental results obtained for the coupling loss are almost independent of the launching conditions due to the strong mode coupling in this fibre. This means that no important mode redistribution takes place



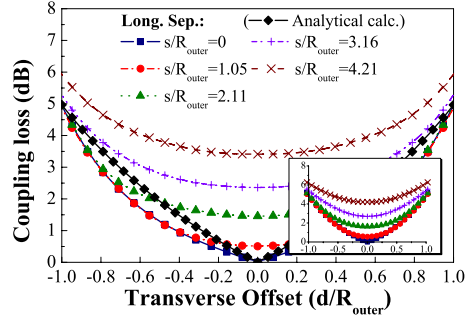
(a) Experimental results with  $NA_{input} = 0.1$ .



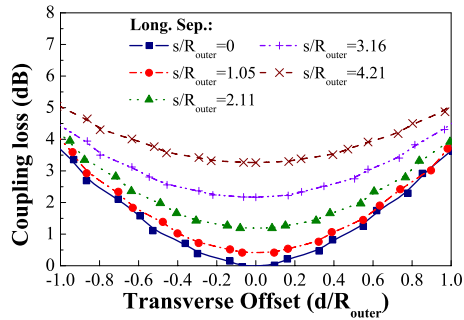
(b) Numerical results with  $NA_{input} = 0.1$ .



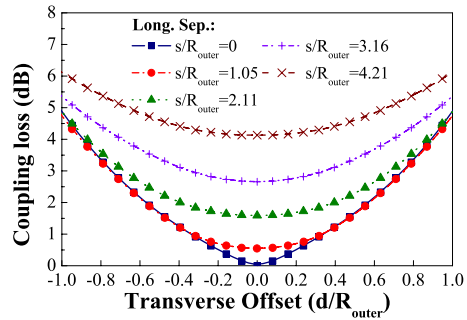
(c) Experimental results with  $NA_{input} = 0.65$ .



(d) Numerical results with  $NA_{input} = 0.65$ .

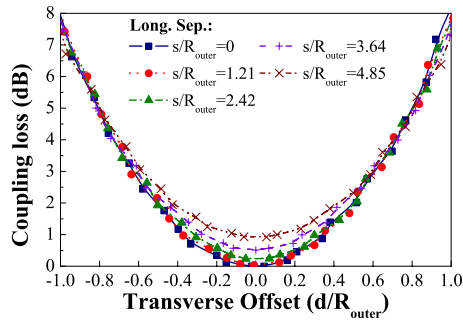


(e) Experimental results with a green LED.

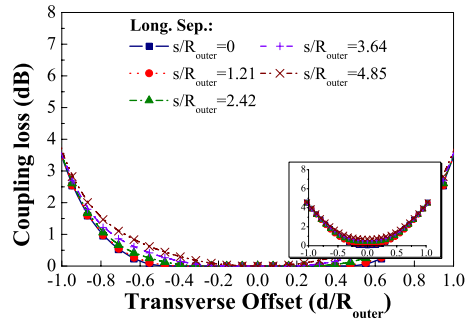


(f) Numerical results with a green LED.

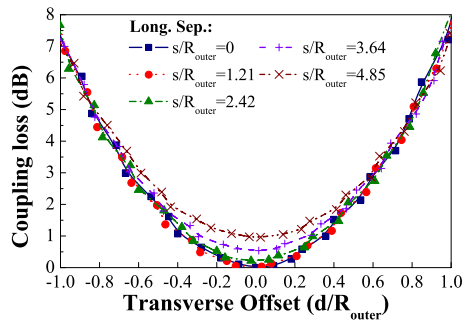
Fig. 11. Eska-Miu fibre. Coupling loss against normalized transverse offset  $d/R_{outer}$  for various longitudinal separations and for different source configurations. Experimental and numerical results. The insets correspond to the results obtained when the source covers the whole input surface of the transmitting fibre. The analytical results denoted by  $\blacklozenge$  are shown superimposed on the numerical results obtained with  $NA_{input} = 0.65$ .



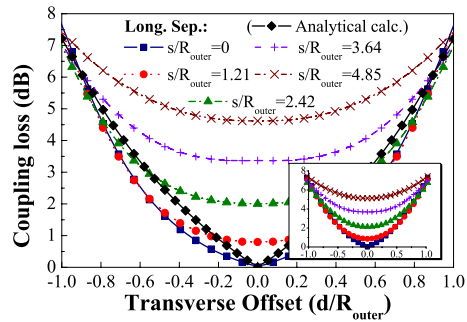
(a) Experimental results with  $NA_{input} = 0.1$ .



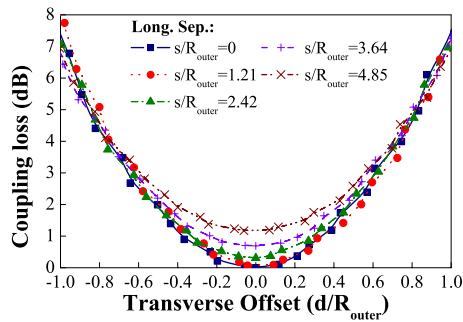
(b) Numerical results with  $NA_{input} = 0.1$ .



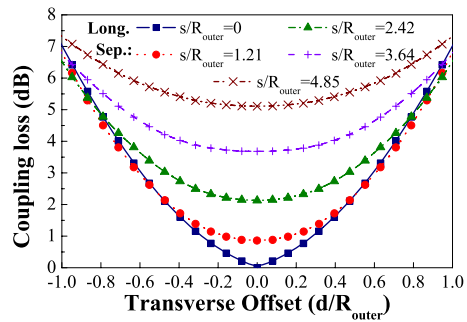
(c) Experimental results with  $NA_{input} = 0.65$ .



(d) Numerical results with  $NA_{input} = 0.65$ .



(e) Experimental results with a green LED.



(f) Numerical results with a green LED.

Fig. 12. TVER fibre. Coupling loss against normalized transverse offset  $d/R_{outer}$  for various longitudinal separations and for different source configurations. Experimental and numerical results. The insets correspond to the results obtained when the source covers the whole input surface of the transmitting fibre. The analytical results denoted by  $\blacklozenge$  are shown superimposed on the numerical results obtained with  $NA_{input} = 0.65$ .

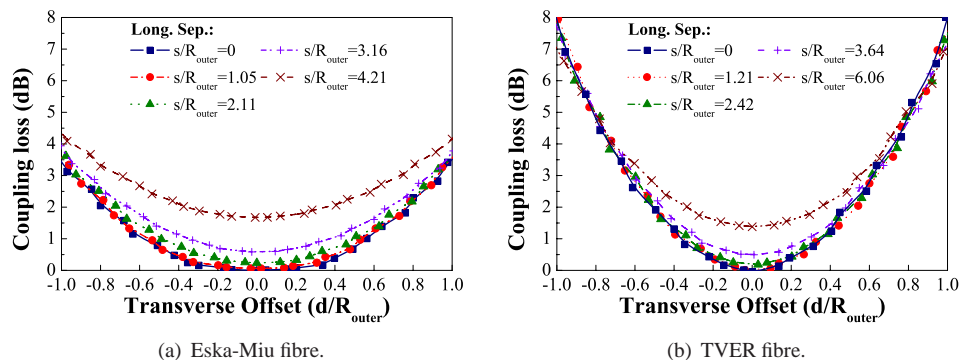


Fig. 13. Coupling loss against normalized transverse offset  $d/R_{outer}$  for various longitudinal separations and using an 8-shaped scrambler in the transmitting fibre ( $NA_{input} = 0.1$ ). Experimental results obtained for the Eska-Miu and TVER fibres.

when changing from one source to another.

Let us now compare the experimental results obtained for both MSI-POFs when using a 0.1-NA red laser diode in combination with an 8-shaped scrambler, which are represented in Figs. 13(a) and 13(b). In the case of the Eska-Miu fibre, a transverse offset equal to the radius of the fibre ( $d/R_{outer} = 1$ ) when there is no longitudinal separation ( $s/R_{outer} = 0$ ) leads to a coupling loss of approximately 3.5 dB. This effect is even more dramatic on the TVER fibre, whose coupling loss turns out to be in the order of 7–8 dB. Another significant parameter is the 3-dB coupling-loss point, which is  $d/R_{outer} = 0.94$  for the Eska-Miu fibre and 0.62 for the TVER one. Indeed, these values are certainly lower than those obtained for longitudinal separations alone, which is indicative of the greater importance of transverse offsets as regards coupling loss. The reasons for such a behaviour have already been discussed at the end of the previous subsection.

On the other hand, as the longitudinal separation between fibres increases, coupling loss increases more and more slowly with the normalized transverse offset, and there is eventually a certain offset value from which greater longitudinal separations produce lower losses. As an example, let us consider the TVER fibre illuminated by a light source with an input numerical aperture of 0.1 through an 8-shaped scrambler (see Fig. 13(b)). In this case, we can observe that, in the absence of longitudinal separation ( $s/R_{outer} = 0$ ), there is an increase of nearly 8 dB in the coupling loss when changing from  $d/R_{outer} = 0$  to  $d/R_{outer} = 1$ . Instead, for a longitudinal separation of  $s/R_{outer} = 6.06$  this increase is reduced to 7.1 dB. This behaviour can be explained on the assumption that the light exiting the transmitting fibre generates a divergent cone of radiation that overlaps the cross-section of the receiving fibre. As this cone is moved along the transverse direction, the power captured inside decreases. The decrease in power is much slower when considering larger longitudinal separations, for which the cross-section of the cone of radiation is bigger, and therefore, the power distribution is smoother.

Finally, as was discussed in the previous subsection, coupling losses due to small transverse offsets ( $d/R_{outer}$  in the vicinity of 0) are higher in the case of the Eska-Miu fibre when considering large longitudinal separations, as a result of the smoother power density of the emitting cone of radiation.

To sum up, the transverse offset has so far proved to be the most critical parameter when dealing with coupling losses for MSI-POFs, just like in SI and GI optical fibres [6, 9].

#### 4.4. Angular misalignment

The experimental and numerical results in Figs. 14 and 15 show the behaviour of coupling loss with an angular misalignment. In those plots where the longitudinal separation appears as a parameter, the measured output power is referring to the power recorded at  $d/R_{outer} = 0$ ,  $s/R_{outer} = 0.53$  (for the Eska-Miu fibre) or  $0.61$  (for the TVER fibre), and  $\alpha = 0^\circ$ . This is our 0-dB reference point. In the other plots where the transverse offset appears as a parameter, the reference position is  $d/R_{outer} = 0$ ,  $s/R_{outer} = 1$ , and  $\alpha = 0^\circ$ .

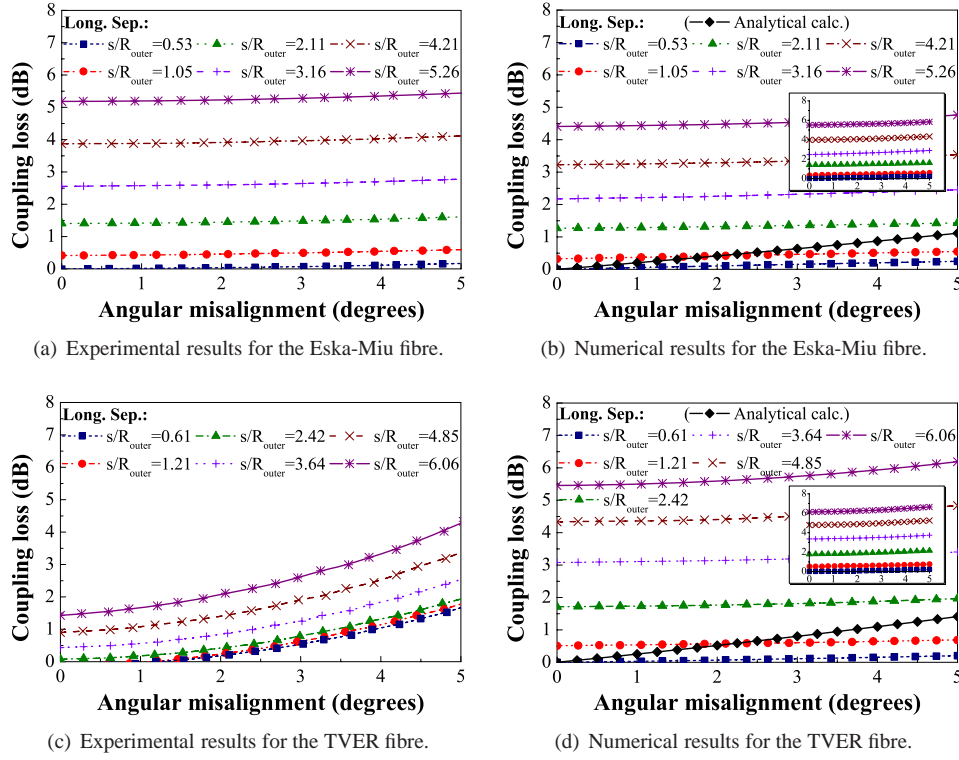


Fig. 14. Coupling loss against angular misalignment  $\alpha$  (in degrees) for various longitudinal separations for an input numerical aperture  $NA_{input} = 0.65$ . Experimental and numerical results. The insets correspond to the results obtained when the source covers the whole input surface of the transmitting fibre. The analytical results denoted by  $\blacklozenge$  are shown superimposed on the numerical results.

The results for coupling losses as a function of the angular misalignment for various longitudinal separations are illustrated in Fig. 14. On the one hand, Fig. 14(a) shows the coupling losses in the case of the Eska-Miu fibre (in which they do depend on light launching conditions) in the least favorable case, namely when the value of the input numerical aperture is  $NA_{input} = 0.65$ . It is clear from Fig. 14(b) that the numerical results shown in the insets are in better agreement with the experimental ones, for the same reasons discussed above. On the other hand, Fig. 14(c) shows the results for the TVER fibre. For this fibre, as happened with both longitudinal separations and transverse offsets, coupling losses due to an angular misalignment are almost independent of the launching conditions, due to mode coupling effects. This makes it difficult to establish any comparison between the experimental results and the numerical ones represented in Fig. 14(d).

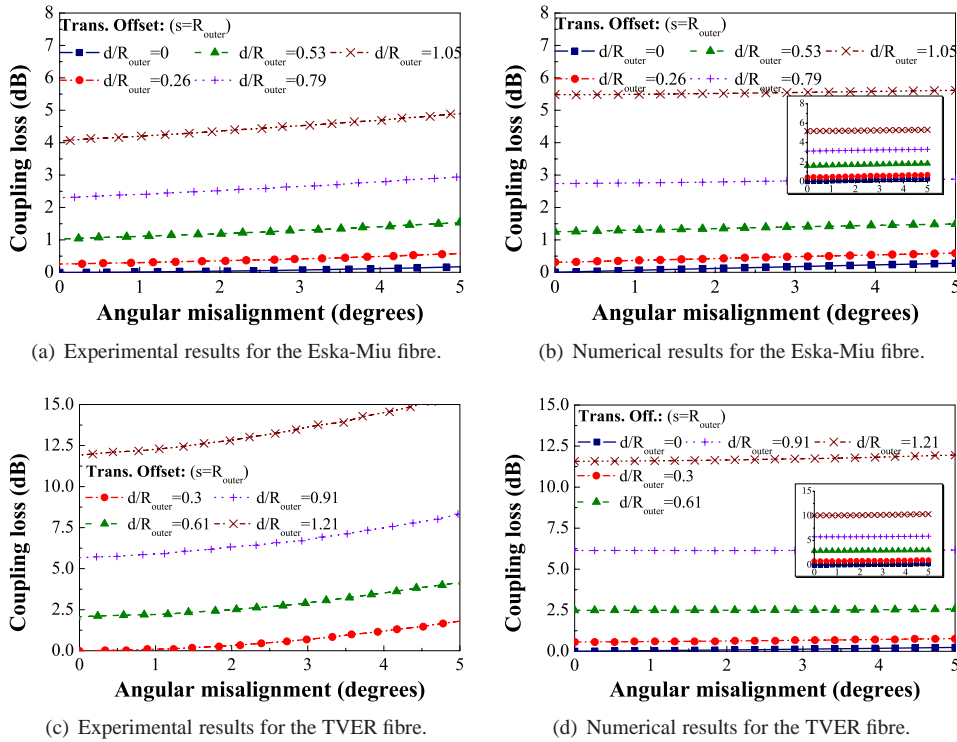


Fig. 15. Coupling loss against angular misalignment  $\alpha$  (in degrees) for various transverse offsets for an input numerical aperture  $NA_{input} = 0.65$ . Experimental and numerical results. The insets correspond to the results obtained when the source covers the whole input surface of the transmitting fibre.

Figure 15 shows, again, coupling losses against angular misalignment, but this time for different transverse offsets. Figures 15(a) and 15(b) correspond to the Eska-Miu fibre, whereas Figs. 15(c) and 15(d) are related to the TVER fibre. It must be pointed out, once more, the high sensitivity to the transverse offset of coupling losses, especially when dealing with the TVER fibre.

In any case, the analytical predictions can be regarded as an upper bound for both fibres, provided that the effects of a transverse offset or a longitudinal separation are discarded.

Finally, in view of the weak dependence shown by coupling losses on angular misalignments, it can be concluded that angular misalignments are not as critical as transverse offsets or longitudinal separations, provided that they are kept sufficiently small. Furthermore, we have found that losses always remain well below 3 dB for practical values of the angular misalignment.

## 5. Conclusion

In this paper we have primarily compared existing and novel analytical models for coupling losses with both numerical computer simulations and experimentally measured data. Our analytical expressions corresponding to coupling losses have been completed in this paper with those corresponding to angular misalignments. In all cases, the formulae were derived under the assumption of a uniform power distribution across the light cone of radiation defined by the input numerical aperture. For this reason, the analytical calculations performed are fairly

pessimistic. However, it has been proved that they are never worse than the results obtained experimentally, so we ensure that the real measurements are well below these limit values. Therefore, we can conclude that the analytical calculations provide an upper bound for coupling losses. Regarding the experimental and numerical results, these have revealed that, in several cases, coupling losses do depend on the mode distribution in the fibre. For instance, the results obtained for the Eska-Miu fibre depend on light launching conditions, whereas this dependence is much weaker in the TVER fibre, due to stronger mode coupling. Finally, in the light of the analytical, numerical and experimental results, it is clear that connector designers should pay close attention to transverse offsets in order to minimize coupling losses.

### Appendix A: Proof of the relationship between transverse offset and angular misalignment

Although the principal ray optics variables such as the ray polar position  $r$  and the axial direction  $\theta_z$  have no physical meaning in the wave optics picture, the combination [5]

$$R^2 = r^2 + \frac{n^2 \sin^2 \theta_z}{n^2 - n_{cl}^2} \quad (A1)$$

is directly related to the propagation constant  $\beta$  of a fibre mode and, therefore, to the ray invariant  $\tilde{\beta}$  [26, 27]. The expression above corresponds to fibres having a clad parabolic profile, although it leads to very accurate results in the case of near square-law profile fibres. The magnitude  $R$  in

$$R^2 = \left(1 - \frac{\beta^2}{k^2 n^2}\right) \frac{n^2}{n^2 - n_{cl}^2} \quad (A2)$$

is the length of a vector in the phase space pointing to the locus of the fibre mode; hence, it is called the mode coordinate. In the equations above,  $k$  is the vacuum wave number and  $n$  the refractive index associated to each layer.

By defining a normalized angular coordinate

$$\sigma = \frac{n \sin \theta_z}{(n^2 - n_{cl}^2)^{1/2}}, \quad (A3)$$

and substituting Eq. (A3) for Eq. (A1)

$$R^2 = r^2 + \sigma^2. \quad (A4)$$

Since  $r$  and  $\sigma$  are interchangeable in this relationship, it can be proved that transverse offsets and angular misalignments can be treated in the same way. Therefore, introducing a single offset variable  $D$  which gathers both the transverse offset  $d$  and the angular misalignment  $\alpha$ , defined as

$$D^2 = d^2 + \frac{n^2 \sin^2 \alpha}{n^2 - n_{cl}^2}, \quad (A5)$$

the coupling loss for an angular misalignment can be easily computed using the same formulae derived for transverse offsets.

### Acknowledgments

The authors would like to thank T. Yamamoto of Mitsubishi Rayon Co., Ltd., and Prof. V. Levin of RPC for supplying the MSI-POF samples.

This work was supported by the *Universidad del País Vasco–Euskal Herriko Unibertsitatea* and the *Ministerio de Ciencia y Tecnología* under projects 9/UPV 00147.345-14626/2002ZUBIA, and TIC2003-08361.